



Available online at www.sciencedirect.com



ScienceDirect

Trans. Nonferrous Met. Soc. China 29(2019) 976–983

Transactions of
Nonferrous Metals
Society of China

www.tnmsc.cn



Microstructure, texture and mechanical properties of Mg–8Gd–4Y–1Nd–0.5Zr alloy prepared by pre-deformation annealing, hot compression and ageing

Yi-ping WU¹, Han-qing XIONG¹, Yu-zhen JIA², Shao-hui XIE¹, Guo-feng LI¹

1. Department of Mechanical and Electrical Engineering, Changsha University, Changsha 410022, China;

2. Bichamp Cutting Technology (Hunan) Co., Ltd., Changsha 410200, China

Received 11 June 2018; accepted 16 November 2018

Abstract: An extruded Mg–8Gd–4Y–1Nd–0.5Zr alloy was pre-heated at 470 °C for 1 h and subsequently compressed at 470 °C and two strain rates of 0.2 and 0.0003 s⁻¹. Microstructure, texture and mechanical properties of the alloy were examined by optical microscopy (OM), scanning electron microscopy (SEM), electron backscatter diffraction (EBSD), hardness test and tensile test. The results show that the post-deformed microstructures of alloy are non-uniform at both strain rates due to the dissolution of RE-rich particles and the occurrence of DRX. The textures of post-deformed alloy are affected by strain rate. The alloy exhibits a strong basal texture of <0001>/ND (normal direction) after compression at 0.2 s⁻¹, while a weak texture component of <0001>/ED (extrusion direction) is formed in the compression obtained at 0.0003 s⁻¹. Compared with the alloy compressed at 0.0003 s⁻¹, the compressed alloy obtained at 0.2 s⁻¹ presents better comprehensive mechanical properties with the ultimate tensile strength of 426 MPa, yield strength of 345 MPa and ductility of 2.1% when being aged at 225 °C for 8 h.

Key words: magnesium alloys; strain rate; microstructure; texture; mechanical properties

1 Introduction

Magnesium alloys with additions of rare-earth (RE) elements, such as Gd and Y, have received tremendous attentions in the automobile and aerospace industries due to their low density and high specific strength [1,2]. New cast Mg–RE alloys have relatively good comprehensive properties after peak ageing, with ultimate tensile strength higher than 300 MPa, yield strength higher than 210 MPa and ductility of 6% [2]. Mg–RE alloys are often subjected to high temperature deformation when non-basal slip systems can be activated [3], and increasing interests are attracted in developing Mg–RE alloys with a good combination of strength and formability by manipulating deformation parameters and heat treatments. The compressed and peak-aged Mg–RE alloy presents an ultimate tensile strength of 416 MPa, a yield strength of 317 MPa, and an elongation of 2.7% [4].

Much work has been done to understand the temperature effect [5–10]. Temperature has a great

impact on the solid solubility of RE elements in Mg matrix which drops quickly with decreasing the temperature [5]. Dynamic precipitation can take place during the hot deformation of Mg–RE alloys at 450 °C [6–8,11], while RE-rich particles will extensively dissolve into the matrix when the deformation temperature is up to 500 °C [9,10]. The interaction between RE-rich particles and the migration of grain boundaries will affect not only dynamic recrystallization behavior [12,13] but also mechanical behavior of Mg–RE alloys [6–10,14]. It is well known that low temperature and high strain rate easily induce a high stress concentration, leading to the formation of voids and further nucleate cracking [15,16]. The flow stress and strain rate sensitivity increased with increasing strain rate during compression of an extruded Mg alloy [17].

Recently, distinct differences in microstructure and texture of a Mg–RE alloy during hot compression at two deformation temperatures and the same strain rate have been reported, which has been attributed to the disparity brought by dynamic precipitation at low temperatures and dynamic dissolution at high temperatures. For more

details, please refer to Ref. [10]. In this work, a Mg–8Gd–4Y–1Nd–0.5Zr (wt.%) alloy has been compressed at 470 °C under two different strain rates. The role of strain rate in the formation of microstructure, texture and mechanical properties has been systematically investigated.

2 Experimental

The extruded Mg–8Gd–4Y–1Nd–0.5Zr (wt.%) plate with dimension of 210 mm × 70 mm × 25 mm was used. Before compression, the plate was pre-heated at 470 °C for 1 h. The compression was finished in one pass along the normal direction (ND) at 470 °C. Two strain rates of 0.2 and 0.0003 s⁻¹ were applied. The final compression strain of was 0.69. After compression, the sample was immediately quenched into cold water.

Microstructural examination was performed by Olympus DP 70 Optical Microscope (OM) and Leo 1530 Field Emission Gun-Scanning Electron Microscope (FEG-SEM). The average grain size of the alloys was obtained using a mean linear intercept method. The average diameter and area fraction of precipitates were calculated using Image J. HKL commercial software was used to determine the textures of samples before and after compression based on the electron backscatter diffraction (EBSD) tests. And all EBSD maps were obtained on planes perpendicular to extrusion direction (ED).

The cylindrical samples with 5 mm in diameter and 30 mm in length along ED were cut for tensile testing at room temperature. Tensile tests were finished on an Instron 50 kN 3369 test machine at a crosshead speed of 1 mm/min. Gauge length of about 25 mm was marked on each tensile sample to measure the elongation after fracture. Three specimens were tested for each condition. The compressed samples were aged at 225 °C for different time. The hardness tests were performed on a HV–10B hardness tester with a load of 29.4 N.

3 Results

3.1 Before compression

3.1.1 Microstructures

Figure 1 shows the microstructure of the pre-heated alloy which displays a uniform grain structure. Its average grain size is ~6 µm. Plenty of irregularly-shaped particles are preferably distributed along grain boundaries (Fig. 1(a)). The area fraction and average diameter of particles are ~6.7% and ~1.1 µm (Fig. 1(b)). The particles in the alloy are most likely Mg₅(Gd,Y) [18,19].

3.1.2 Micro-texture

EBSD results of the pre-heated alloy are presented

in Fig. 2. In the orientation map (Fig. 2(a)), thin white line represents low-angle grain boundaries (LAGBs, grain boundaries misorientation ≤15°) and thick black line indicates high-angle grain boundaries (HAGBs, grain boundaries misorientation >15°). The complete

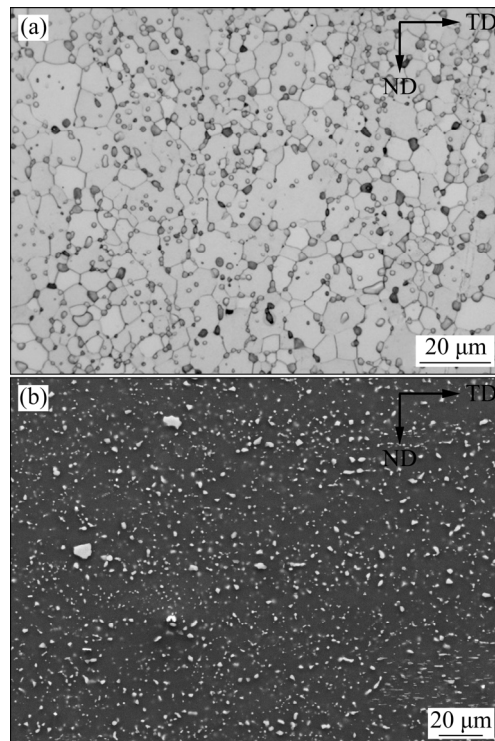


Fig. 1 Microstructure of pre-heated alloy: (a) OM image; (b) SEM image

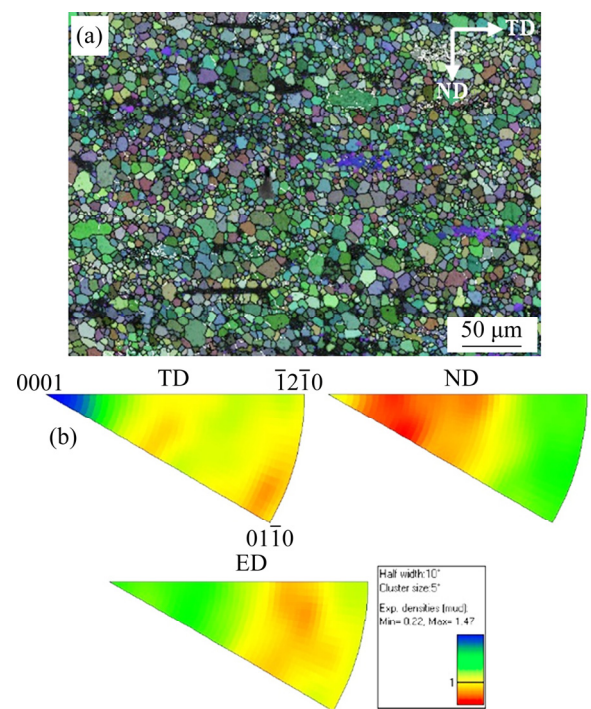


Fig. 2 EBSD results of pre-heated alloy: (a) Orientation map; (b) Inverse pole figures (IPFs)

dark areas in Fig. 2(a) are unindexed points during EBSD scanning. As seen, equiaxed grains dominate in the microstructure of the pre-heated alloy, with few LAGBs detected in several large grains. Figure 2(b) gives the corresponding inverse pole figures (IPFs). The alloy principally orientates with *c*-axes of grains parallel to ND. The texture is pretty weak with the maximum intensity of 1.47.

3.2 After compression

3.2.1 Microstructures

Figure 3(a) shows the microstructures of the alloy compressed at 470 °C and strain rate of 0.2 s⁻¹. The alloy presents a rather broad grain size distribution. Some large grains and extra-coarse particles are elongated parallel to TD. Grains are extra-large when fewer particles are distributed around them due to the lack of pinning. Figure 3(b) exhibits the microstructure of the alloy compressed at 470 °C and strain rate of 0.0003 s⁻¹. The above-mentioned large long grains are not observed. Equiaxed grains dominate in the microstructure. Particles are distributed more randomly in this alloy. As seen in Fig. 3, both the grain structure and the distribution of particles of the compressed samples become heterogeneous after compression at 470 °C. Some long grains with less particles pinned around appear in the compressed alloys.

Figure 4 shows the SEM images of the compressed alloys to observe the morphology and distribution of

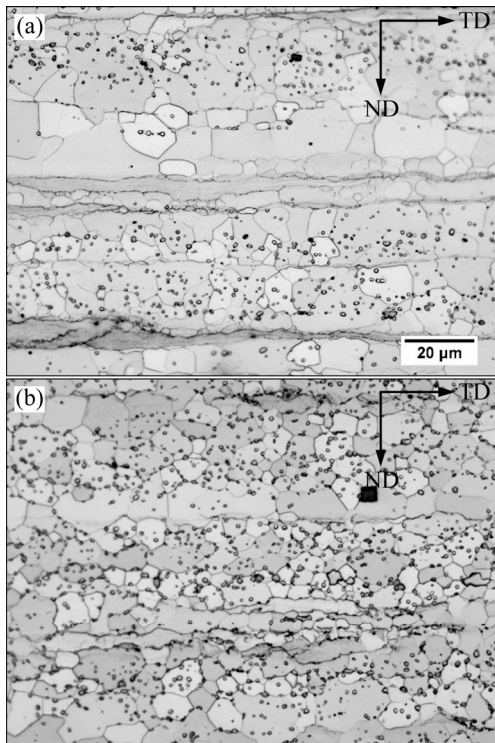


Fig. 3 OM images of alloys compressed in different conditions: (a) 470 °C, 0.2 s⁻¹; (b) 470 °C, 0.0003 s⁻¹

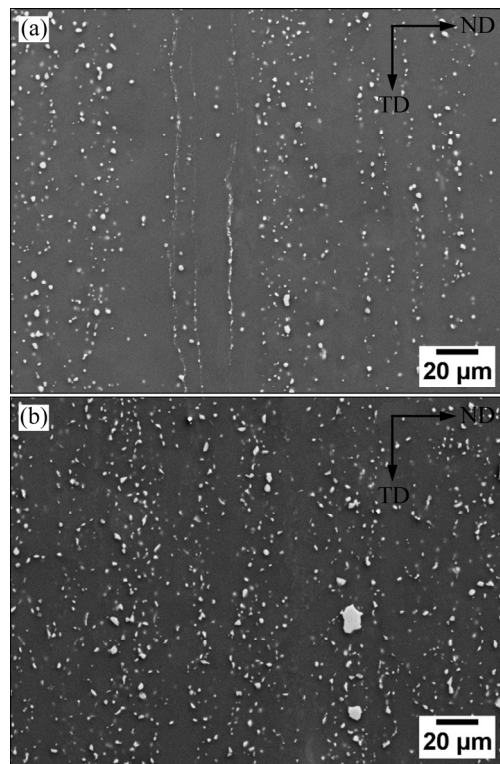


Fig. 4 SEM images of alloys compressed in different conditions: (a) 470 °C, 0.2 s⁻¹; (b) 470 °C, 0.0003 s⁻¹

particles. As observed, the coarse particles are irregularly shaped, and they have a slight trend to align along TD. The area fraction and average diameter of the particles are calculated. During compression, particles become to dissolve into the matrix. Specifically, the area fraction and average diameter of particles in the sample compressed at 470 °C and 0.2 s⁻¹ are ~3.6% and ~1.2 µm, respectively, close to ~3.9% and ~1.4 µm of the sample compressed at 470 °C and 0.0003 s⁻¹.

3.2.2 Micro-texture

Figure 5 presents EBSD results of the compressed samples. Orientation maps (Figs. 5(a) and (b)) show more details in grain size distribution. Figure 5(a) exhibits the non-uniform grain structure of the sample compressed at 470 °C and strain rate 0.2 s⁻¹. Bands of fine grains form between bands of large grains. Moreover, the bulging of grain boundaries is obvious, indicating the occurrence of discontinuous dynamic recrystallization (DDRX) during compression. In addition, one isolated fine grain forms inside a large grain (as arrowed in Fig. 5(a)), and this may result from the particle stimulated nucleation (PSN) due to the presence of RE-rich particles. Figure 5(b) shows a district of relatively equiaxed grains in the sample compressed at 470 °C and strain rate of 0.0003 s⁻¹, with some extra-large grains surrounded by numbers of small grains. DDRX has also occurred according to the apparent grain

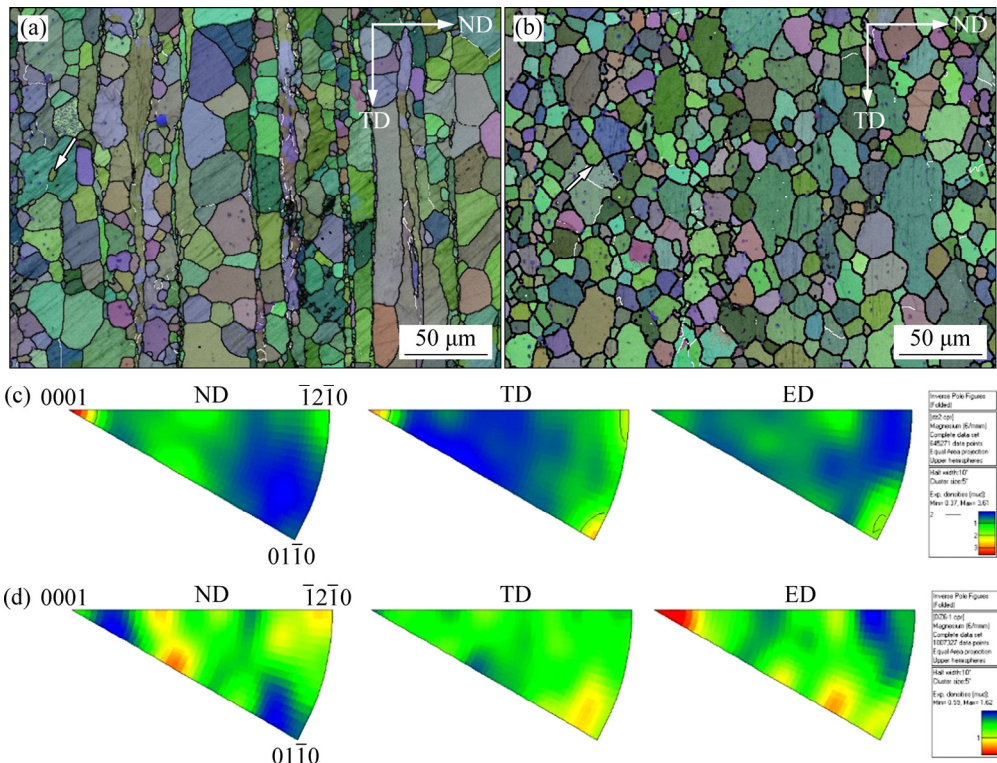


Fig. 5 EBSD orientation maps (a, b) and inverse pole figures (c, d) of alloys compressed in different conditions: (a, c) 470°C , 0.2 s^{-1} ; (b, d) 470°C , 0.0003 s^{-1}

boundary bulging (as arrowed in Fig. 5(b)).

The corresponding inverse pole figures are shown in Figs. 5(c) and (d) which show distinct texture components of the compressed samples. Figure 5(c) depicts a strong texture type of $\langle 0001 \rangle // \text{ND}$ (normal direction) with the maximum intensity of 3.61 in sample compressed at 470°C and strain rate of 0.2 s^{-1} . C-axes of grains are principally orientated parallel to ND. For the sample compressed at 470°C and strain rate of 0.0003 s^{-1} , a weak texture component is distinguished as $\langle 0001 \rangle // \text{ED}$ (extrusion direction) with the maximum intensity of 1.62 in Fig. 5(d).

3.2.3 Ageing behavior

The age-hardening behavior of the compressed samples is shown in Fig. 6. It is seen that, the two compressed alloys present almost the same original hardness values of HV 85.6 and HV 84.3, respectively. However, the compressed alloy obtained at the strain rate of 0.2 s^{-1} shows a slightly higher level of hardenability than the alloy obtained at 0.0003 s^{-1} , and it is interesting to notice that two samples reach the same peak hardness value of HV ~ 126 after 12 h ageing.

3.2.4 Mechanical properties

The tensile properties including yield strength (YS), ultimate tensile strength (UTS) and ductility (δ) of the compressed samples are presented in Fig. 7. Obviously, the compressed sample obtained at the strain rate of

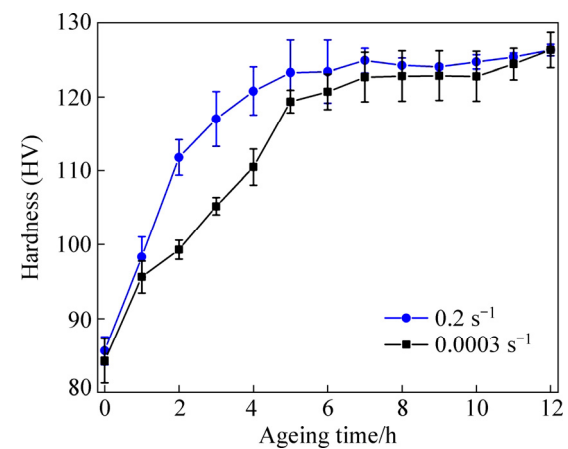


Fig. 6 Ageing hardening response of compressed samples with ageing time

0.2 s^{-1} shows better comprehensive mechanical properties than those of the compressed sample obtained at the strain rate of 0.0003 s^{-1} . YS, UTS and δ of the former sample are 247 MPa, 307 MPa and 10%, respectively. As seen in the ageing hardening curve in Fig. 6, the compressed alloy has almost arrived the highest hardness after ageing for 8 h and the hardness value is very steady during 7–10 h ageing. Thus, the 8 h aged samples have been chosen which are expected to present the best comprehensive properties. After ageing

at 225 °C for 8 h, the strengths are greatly enhanced with YS of 345 MPa and UTS of 426 MPa. Note that the strengths of the compressed sample obtained at the strain rate of 0.0003 s⁻¹ are not improved too much after 8 h ageing, but the ductility drops a lot, from 9.5% to 1.4%.

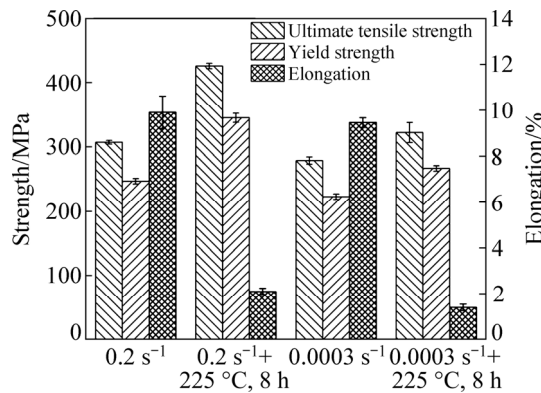


Fig. 7 Mechanical properties of compressed samples at room temperature (Results shown are averages of three tests)

4 Discussion

4.1 Microstructural evolution

The equilibrium Mg₅(Gd,Y) phase was sensitive to deformation temperature. In the compression temperature range of 300–400 °C, the phase precipitation took place, whereas it did not occur when the temperature exceeded 450 °C [8]. In the present study, the relatively high compression temperature of 470 °C leads to the dissolution of Mg₅(Gd,Y) phase during compression, subsequently weakening the inhibition of grain boundary motion and promoting grain growth, which has been verified in Fig. 3. In the compressed samples, the particle features including area fraction and average diameter close to each other also indicate that the evolution of particles is mostly influenced by the deformation temperature rather than strain rate.

As seen in Figs. 1 and 2, the pre-heated sample shows a microstructure of equiaxed grains due to static recrystallization. During compression at 470 °C, DRX becomes active to affect the compressed microstructures. The average grain sizes of the compressed samples are larger than those of the pre-heated sample with the occurrence of DRX and the dissolution of RE particles. In fact, DDRX is observed during compression in Fig. 5. During DDRX process, new grains nucleate preferentially at the original grain boundaries by grain boundary bulging due to strain-induced boundary migration [20]. One compressed sample was obtained at the strain rate of 0.2 s⁻¹ which is three orders of magnitude larger than the sample obtained at 0.0003 s⁻¹, so its compression process was finished much faster than the latter. Therefore, there may be no enough time for

diffusion to take place. The case that some grains can absorb more energies than some others happens more often in the former compressed sample, leading to a bimodal grain structure distribution composed of extra-fine DRX grains and coarse DRX grains, as seen in Fig. 5(a). Such a bimodal microstructure resulted from hot deformation of Mg alloys was reported in other studies as well [21,22]. The decreasing inhibition from RE particles can amplify the phenomenon. Furthermore, since the latter compressed sample was formed at 470 °C and 0.0003 s⁻¹, which can be supposed as a kind of superplastic deformation when the deformation mechanisms of grain boundary sliding (GBS) and grain boundary diffusion generally participate. It has been experimentally demonstrated for both Mg alloys and Al alloys that GBS can be activated at low strain rates [19,23,24]. GBS can be aided by grain boundary diffusion and the importance of grain boundary diffusion increases with decreasing strain rate [25–27]. Hence, for the latter compressed sample, its grain structure may result from DDRX and PSN, and is decorated with equiaxed grains also due to superplastic deformation.

4.2 Effect of strain rate on texture evolution

The addition of RE elements can significantly modify and weaken the deformation texture of Mg alloys [28–30]. In a previous work, the studied alloy was pre-heated at 500 °C for 0.5 h and subsequently compressed under three conditions of 500 °C, 0.2 s⁻¹, 450 °C, 0.2 s⁻¹ and 450 °C, 0.0003 s⁻¹. It was found that the further dissolution of particles into the matrix during compression contributed to the formation of a normal basal texture component in the compressed alloy. Nevertheless, the occurrence of dynamic precipitation during compression induced severe pinning effect, leading to random and weak textures [10]. The present work further exhibits the effect of strain rate on texture in the dynamic dissolution state. In the compressed sample (470 °C, 0.2 s⁻¹), the non-uniform release of deformation energy causes heterogeneous grain size distribution, which brings about the anisotropy and a relatively strong texture. The formation of the compressed sample (470 °C, 0.0003 s⁻¹) is similar as a kind of superplastic deformation, and the related deformation mechanisms generally result in random alignments of equiaxed grains, i.e., weak texture. DDRX and PSN mechanisms also contribute to the texture evolution, but both result in random textures during hot deformation of Mg alloys [31]. Therefore, the former compressed sample exhibits a strong basal texture of <0001>/ND (Fig. 5(c)) which has also been explained in Ref. [10], while the maximum texture intensity of the latter compressed sample is 1.62. Also, another texture component of <1121>/ED is detected, which is known to be a

recrystallization effect due to orientations appearing in RE containing Mg alloys [30].

4.3 Effect of strain rate on mechanical properties

The hardness values of the compressed sample at 470 °C, 0.2 s⁻¹ are slightly higher than those of the compressed sample at 470 °C, 0.0003 s⁻¹ with the same ageing time. Considering the same alloying chemistry and similar particle features, the similar hardening rates are expected. However, the presented ageing behavior in Fig. 6 does not accord with the expectation. In the first 2 h ageing, the hardening rate of the former compressed sample is higher than that of the latter compressed sample. With ageing time increasing to the second stage of 2–5 h, the hardening rate of the latter compressed sample is beyond that of the former compressed sample in turn. And finally, the two hardening rates are close to each other, and the discrepancy becomes tinier with increasing ageing time increasing from 5 to 12 h. As shown in Fig. 3, although the particle features of the compressed samples are very similar, the former compressed sample still has a ~0.3% area fraction less than the latter. Furthermore, as seen in Figs. 5(a) and (b), a higher fraction of LAGBs are observed in the former than in the latter, which is reasonable if we consider the different strain rates employed in the two samples. Thus, the former can show higher hardness values than the latter at the same ageing time because of a little bit lower area fraction of particles precipitated. But with sufficient ageing time, both samples can gain strong strengthening effects, such as the same peak value at 12 h. Ageing cannot change the grain structure due to its low temperature, but it is facilitated for the disappearance of substructures in samples. This further accounts for the continuous declination of hardening rate of the former.

Figure 4 displays that microstructures of both compressed samples are not as uniform as that of the pre-heated sample in Fig. 2, and Fig. 5 shows more details of grain structures in the compressed samples. The compressed sample (470 °C, 0.2 s⁻¹) consists of bands of extra-fine grains and bands of coarse grains. A way to improve the ductility of alloys is producing a bimodal microstructure. In a somewhat simplistic view, coarse grains provide enhanced ductility and ultra-fine/nano grains were responsible for high strength [32]. Furthermore, according to the textures of the compressed samples in Figs. 5(c) and (d), such texture in the compressed sample (470 °C, 0.0003 s⁻¹) restricts the availability of potentially active basal slip during tensile testing along ED at room temperature. Therefore, the latter compressed sample may break earlier than the former, which is detrimental for both ductility and strengths. The comprehensive mechanical properties of the latter compressed sample are even worse than those

of the former compressed sample after the same ageing treatment (225 °C, 8 h).

5 Conclusions

(1) The average grain sizes of the compressions are larger than those of the pre-heated sample due to the dissolution of RE-rich particles and the occurrence of DRX during compression. Due to its feature of superplastic deformation, the sample forming at the strain rate of 0.0003 s⁻¹ presents a more uniform microstructure than the sample obtained at the strain rate of 0.2 s⁻¹.

(2) The textures after compression are different with changing strain rate. A strong basal texture component of <0001>/ND is formed in the compressed sample obtained at 470 °C, 0.2 s⁻¹, while a weak texture component of <0001>/ED is detected in the sample obtained at 470 °C, 0.0003 s⁻¹.

(3) The compressed sample obtained at 470 °C, 0.2 s⁻¹ shows better comprehensive mechanical properties than the compressed sample obtained at 470 °C, 0.0003 s⁻¹. After ageing at 225 °C for 8 h, the yield strength, ultimate tensile strength and ductility of the former sample can achieve 345 MPa, 426 MPa and 2.1%, respectively.

Acknowledgments

The authors gratefully acknowledge the financial support from the Changsha University Talent Introduction Project (50800-92808) and the Changsha Science and Technology Project (K1705055). The present work was also carried out with the support of the Advanced Characterization Facility in Waurn Ponds Campus of Deakin University, Geelong, Victoria, Australia.

References

- [1] TANG Chang-ping, WU Kai, LIU Wen-hui, FENG Di, WANG Xue-zhao, MIAO Guo-dong, ANG Mao-mao, LIU Xiao, QUAN Li. Effects of Gd, Y content on the microstructure and mechanical properties of Mg–Gd–Y–Nd–Zr alloy [J]. Metals, 2018, 8: 790–800.
- [2] LI Guo-qiang, ZHANG Jing-huai, WU Rui-zhi, FENG Yan, LIU Shu-juan, WANG Xiao-jun, JIAO Yu-feng, YANG Qiang, MENG Jian. Development of high mechanical properties and moderate thermal conductivity cast Mg alloy with multiple RE via heat treatment [J]. Journal of Materials Science & Technology, 2018, 34(7): 1076–1084.
- [3] XIA Xiang-sheng, ZHANG Kui, LI Xing-gang, MA Ming-long, LI Yong-jun. Microstructure and texture of coarse-grained Mg–Gd–Y–Nd–Zr alloy after hot compression [J]. Materials & Design, 2013, 44: 521–527.
- [4] WU Yi-ping, ZHANG Xin-ming, DENG Yun-lai, TANG Chang-ping. Microstructure, texture, and enhanced mechanical properties of an extruded Mg–rare earth alloy after hot compression [J]. Journal of

Materials Research, 2015, 30: 3776–3783.

[5] GUO Yong-chun, LI Jian-ping, LI Jin-shan, ZHONG Yang, ZHAO Juan, FENG Xia, LIANG Min-xian. Mg–Gd–Y system phase diagram calculation and experimental clarification [J]. *Journal of Alloys and Compounds*, 2008, 450: 446–451.

[6] HOMMA T, KUNITO N, KAMADO S. Fabrication of extraordinary high-strength magnesium alloy by hot extrusion [J]. *Scripta Materialia*, 2009, 61: 644–647.

[7] CHEN Z B, LIU Chu-ming, XIAO Hong-chao, WANG J K, CHEN Z Y, JIANG Shu-nong, SU Z J. Effect of rolling passes on the microstructures and mechanical properties of Mg–Gd–Y–Zr alloy sheets [J]. *Materials Science and Engineering A*, 2014, 618: 232–237.

[8] XIAO Hong-chao, TANG Bei, LIU Chu-ming, GAO Yong-hao, YU Shi-lun, JIANG Shu-nong. Dynamic precipitation in a Mg–Gd–Y–Zr alloy during hot compression [J]. *Materials Science and Engineering A*, 2015, 645: 241–247.

[9] TANG Lie-chong, LIU Chu-ming, CHEN Zhi-yong, JI Da-wei, XIAO Hong-chao. Microstructures and tensile properties of Mg–Gd–Y–Zr alloy during multidirectional forging at 773 K [J]. *Materials & Design*, 2013, 50: 587–596.

[10] WU Yi-ping, ZHANG Xin-ming, DENG Yun-lai, TANG Chang-ping, ZHONG Ying-ying. Effect of compression conditions on the microstructure and texture of a Mg–RE alloy [J]. *Materials Science and Engineering A*, 2015, 644: 152–158.

[11] ASQARDOUST S H, ZAREI-HANZAKI A, FATEMI S M, MORADJOY-HAMEDANI M. High temperature deformation behavior and microstructural evolutions of a high Zr containing WE magnesium alloy [J]. *Journal of Alloys and Compounds*, 2016, 40: 108–116.

[12] ZHANG J, CHEN B Q, LIU C P. An investigation of dynamic recrystallization behavior of ZK60-Er magnesium alloy [J]. *Materials Science and Engineering A*, 2014, 612: 253–266.

[13] WU Yi-ping, ZHANG Xin-ming, DENG Yun-lai, TANG Chang-ping, YANG Liu, ZHONG Ying-ying. Dynamic recrystallization mechanisms during hot compression of Mg–Gd–Y–Nd–Zr alloy [J]. *Transactions of Nonferrous Metals Society of China*, 2015, 25: 1831–1839.

[14] LI Rong-guang, ZHANG Jing-huai, FU Guan-yan, ZONG Lin, GUO Bei-tao, YU Yong-mei, SU Yong, HAO Yong-sheng. Different precipitation hardening behaviors of extruded Mg–6Gd–1Ca alloy during artificial aging and creep processes [J]. *Materials Science and Engineering A*, 2018, 715: 186–193.

[15] LI Li, ZHANG Xin-ming. Hot compression deformation behavior and processing parameters of a cast Mg–Gd–Y–Zr alloy [J]. *Materials Science and Engineering A*, 2011, 528: 1396–1401.

[16] PENG W P, LI P J, ZENG P, LEI L P. Hot deformation behavior and microstructure evolution of twin-roll-cast Mg–2.9Al–0.9Zn alloy: A study with processing map [J]. *Materials Science and Engineering A*, 2008, 494: 173–178.

[17] GUO Chun-huan, JIANG Feng-chun, WU Rui-zhi, ZHANG Mi-lin. Effect of strain rate on compressive mechanical properties of extruded Mg–8Li–1Al–1Ce alloy [J]. *Materials & Design*, 2013, 49: 110–115.

[18] WU Yi-ping, ZHANG Xin-ming, DENG Yun-lai, TANG Chang-ping, ZHONG Ying-ying. Effect of secondary extrusion on the microstructure and mechanical properties of a Mg–RE alloy [J]. *Materials Science and Engineering A*, 2014, 616: 148–154.

[19] LI Li, ZHANG Xin-ming, DENG Yun-lai, TANG Chang-ping. Superplasticity and microstructure in Mg–Gd–Y–Zr rolled sheet [J]. *Journal of Alloys and Compounds*, 2009, 485: 295–299.

[20] YI S, BROKMEIER H G, LETZIG D. Microstructural evolution during the annealing of an extruded AZ31 magnesium alloy [J]. *Journal of Alloys and Compounds*, 2010, 506: 364–371.

[21] HADADZADEH A, MOKDAD A, AMIRKHIZ B S, WELLS M A, WILLIAMS B W, CHEN D L. Bimodal grain microstructure development during hot compression of a cast-homogenized Mg–Zn–Zr alloy [J]. *Materials Science and Engineering A*, 2018, 724. DOI: <https://doi.org/10.1016/j.msea.2018.03.112>.

[22] KARPARVARFARD S M H, SHAHA S K, BEHRAVESH S B, JAHED H, WILLIAMS B W. Microstructure, texture and mechanical behavior characterization of hot forged cast ZK60 magnesium alloy [J]. *Journal of Materials Science & Technology*, 2017, 33: 907–918.

[23] SABIROV I, ESTRIN Y, BARNETT M R, TIMOKHINA I, HODGSON P D. Enhanced tensile ductility of an ultra-fine-grained aluminum alloy [J]. *Scripta Materialia*, 2008, 58: 163–166.

[24] SABIROV I, ESTRIN Y, BARNETT M R, TIMOKHINA I, HODGSON P D. Tensile deformation of an ultrafine-grained aluminium alloy: Micro shear banding and grain boundary sliding [J]. *Acta Materialia*, 2008, 56: 2223–2230.

[25] WEI Yu-jie, BOWER ALLAN F, GAO Hua-jian. Enhanced strain-rate sensitivity in fcc nanocrystals due to grain-boundary diffusion and sliding [J]. *Acta Materialia*, 2008, 56: 1741–1752.

[26] MARA N A, SERGEEVA A V, MARA T D, MCFADDEN S X, MUKHERJEE A. K. Superplasticity and cooperative grain boundary sliding in nanocrystalline Ni3Al [J]. *Materials Science and Engineering A*, 2007, 463: 238–244.

[27] KUMAR PRAVEEN, XU Cheng, LANGDON TERENCE G. The significance of grain boundary sliding in the superplastic Zn–22% Al alloy after processing by ECAP [J]. *Materials Science and Engineering A*, 2005, 410–411: 447–450.

[28] STANFORD N, BARNETT M R. Effect of composition on the texture and deformation behaviour of wrought Mg alloys [J]. *Scripta Materialia*, 2008, 58: 179–182.

[29] BOHLEN J, NÜRNBERG M R, SENN J W, LETZIG D, AGNEW S R. The texture and anisotropy of magnesium–zinc–rare earth alloy sheets [J]. *Acta Materialia*, 2007, 55: 2101–2112.

[30] STANFORD N, BARNETT M R. The origin of “rare earth” texture development in extruded Mg-based alloys and its effect on tensile ductility [J]. *Materials Science and Engineering A*, 2008, 496: 399–408.

[31] BALL E A, PRANGNELL P B. Tensile-compressive yield asymmetries in high strength wrought magnesium alloys [J]. *Scripta Metallurgica et Materialia*, 1994, 31: 111–116.

[32] HAN B O, LAVERNIA E J, LEE Z, NUTT S, WITKIN D. Deformation behavior of bimodal nanostructured 5083 Al alloys [J]. *Metallurgical and Materials Transactions A*, 2005, 36: 957–965.

经变形前退火、热压缩和时效处理后的 Mg–8Gd–4Y–1Nd–0.5Zr 合金的组织、织构和力学性能

吴懿萍¹, 熊汉青¹, 贾寓真², 谢邵辉¹, 李国锋¹

1. 长沙学院 机电工程学院, 长沙 410022;
2. 湖南泰嘉新材料科技股份有限公司, 长沙 410200

摘要: 挤压态 Mg–8Gd–4Y–1Nd–0.5Zr 合金在 470 °C 下退火 1 h 后, 进行压缩变形, 压缩变形温度为 470 °C, 变形速率为 0.2 s⁻¹ 和 0.0003 s⁻¹。采用金相显微镜(OM)、扫描电镜(SEM)、背散射电子衍射(EBSD)、硬度测试和拉伸试验研究合金的显微组织、织构和力学性能。结果表明: 合金在压缩变形过程中发生富稀土相回溶以及动态再结晶, 导致合金在两种变形速率压缩变形后的组织变得不均匀。压缩态合金的织构受应变速率的影响, 在应变速率为 0.2 s⁻¹ 时, 压缩态合金呈现出强的基面织构(0001)//ND(法向); 而在应变速率为 0.0003 s⁻¹ 时, 合金呈现出弱的织构(0001)//ED(挤压方向)。应变速率为 0.2 s⁻¹ 时获得的合金的综合力学性能更优, 在 225 °C 时效 8 h 处理后, 其抗拉强度达 426 MPa, 屈服强度达 345 MPa, 伸长率达 2.1%。

关键词: 镁合金; 应变速率; 显微组织; 织构; 力学性能

(Edited by Bing YANG)